NUMERICAL STUDY OF GEOMETRIC CHARACTERISTICS OF HELICAL PILES SUBJECTED TO UPLIFT

Plênyo N. G. Araújo
plenyo.araujo@gmail.com
João P. S. Costa
joaopaulodsc@gmail.com
Yuri D. J. Costa
ydjcosta@ct.ufrn.br
Affiliation
Federal University of Rio Grande do Norte
Main Campus, 59078-970, PO box 1524, Natal, Rio Grande do Norte, Brazil.

Abstract. *This paper presents results of numerical simulations of steel helical screw piles subjected to uplift loading, installed in a sedimentary sand deposit. The models have been validated against results of full-scale field tests. The numerical model was built using a finite element code. Analyses were performed to evaluate the effects caused by variations of spacing between helices, helix diameter and depth of installation. Evaluation of failure mechanisms developed in the soil mass surrounding the pile was made possible. Results showed that the transition from shallow to deep anchor conditions is achieved with a ratio between installation depth and average helix diameter of around four. Failure of shallower installations resembles a cylindrical shear failure mode, while failure of deeper installations resembles an individual bearing plate failure mode. Enlarging helix mean diameter results in a linear increase of soil-pile uplift capacity. Increasing inter-helix spacing ratio causes the load to transfer from the top helix to the lower helices and an augment in the uplift capacity. Developing failure mechanisms changes from cylindrical shear to individual plate failure as space ratio is increased. Piles with spacing ratios under 2.8 exhibited shallow anchor behavior.*

Keywords: *Helical pile, Finite element method, Load test, Sand*

1. INTRODUCTION

Steel helical pile foundations have been used in Brazil since the 1990s, mostly in the construction of towers for power transmission and telecommunications (Tsuha, 2007). Despite their advantages over current foundation solutions, the use of helical piles has yet to gain widespread acceptance from the local industry.

Studies on helical anchors are scarce in Brazil and, although the design methodology for helical piles is already well established internationally, information about inspection and monitoring of helical piles is still scarce in the technical literature (Pack, 2003). Procedures to control pile load capacity used in current practice are based on empirical rules established by limited experience of contractors.

The main objective of this paper is to study the load-displacement behaviour of helical piles subjected to uplift loads in a pure sand deposit. The influence of specific geometric variables on the foundation load capacity is assessed. This investigation involved the development of a finite element method (FEM) numerical model, which was validated against tests with helical piles conducted in the field.

2. BACKGROUND

Anchors are foundation systems designed to resist tensile loads and are classified into three types (Kulhawy, 1985):

- Plate anchor: A plate anchor is a rod which transfers the loads to a plate located at the bottom of an excavation backfilled with well compacted material. The plate can be made of steel, concrete, or wood.
- Injected anchor: An injected anchor consists of a cable or steel rod inserted inside an excavation filled with grout.
- Helical pile: A helical pile is a steel shaft to which helical plates are welded. It is installed by screwing into the soil.

Stephenson (2002) reports that modern helical piles are built using circular steel plates welded to tubes. The plates are shaped as a helix with a pitch between edges to minimize soil disturbance. Piles can have more than one helix if proper spacing is kept between them. The central shaft is used to resist the installation torque during installation and to transfer axial loads to the helices.

Helical piles have unique advantages as compared to conventional foundation systems (Perko, 2009; Spagnoli, 2013). Helical piles can be removed and reinstalled, which is an ideal feature for temporary applications or when the pile is installed in a wrong location and needs reinstallation. The installation process is extremely fast and does not leave excavation spoil. During installation, helical piles do not cause excessive vibrations or loud noises. Also, unlike concrete, helical piles do not require a curing time and can be loaded immediately after installation.

According to Perko (2009), the main methods for estimating the uplift load capacity of helical piles are: (1) the cylindrical shear method; (2) the individual bearing method; and (3) the installation torque method. The first two methods are theoretical while the last is based on empirical correlations.

The cylindrical shear method assumes the development of a cylindrical failure surface between the top and bottom helices. The soil between the helices is assumed to behave similarly to a pile, with shearing occurring around the interface. The failure surface above the top helix

Proceedings of the XXXVIII Iberian Latin-American Congress on Computational Methods in Engineering
P.O. Faria, R.H. Lopez, L.F.F. Miguel, W.J.S. Gomes, M. Noronha (Editores), ABMEC, Florianópolis, SC, Brazil, November 5-8, 2017.

has a cone shape, and reaches the soil surface at an angle to the vertical proportional to the angle of internal friction of the soil (Das, 1990).

The depth of the pile influences the failure mode (Das, 1990). The cylindrical shear method considers two possibilities for the failure mechanism that develop in the soil surrounding the pile, which will depend on the ratio between the depth and the diameter of the upper helix (H_1/D_1). Shallow anchor conditions occur when the top helix lies near the soil surface. A conical failure surface develops above the top helix and reaches the surface. Deep anchor conditions occur when the top helix is at a greater depth, and the conical failure surface does not reach the surface. There is a critical H_1/D_1 ratio that represents the transition between shallow and deep conditions. According to Mitsch and Clemence (1985), helical anchors with $H_1/D_1 > 5$ behave as deep anchors in sands with relative density between 44% and 90%.

The uplift load capacity (Q_u) of shallow anchors in sand is calculated using Eq. (1) (Mitsch and Clemence, 1985). Q_u is given by the sum of the friction resistance on the cylindrical surface between the helices and the resistance above the top helix.

$$Q_u = Q_p + Q_f \tag{1}$$

Where:
Q_p = strength developed above the upper helix;
Q_f = friction strength developed on the cylindrical surface formed between the upper and the lower helices.

For deep helical piles in sand, the uplift load capacity is as follows (Mitsch and Clemence, 1985):

$$Q_u = Q_p + Q_f + Q_s \tag{2}$$

Where:
Q_p = strength developed above the upper helix;
Q_f = friction strength developed on the cylindrical surface formed between the upper and the lower helices.
Q_s = friction strength developed on the interface between the pile shaft and the soil above the upper helix.

The individual bearing method according assumes the failure mechanism develops above each helix individually (Clemence et al., 1994). The uplift capacity of the pile is the sum of the individual capacities of the n helices with the friction resistance along the length of the shaft, and can be calculated using Eq. (3).

$$Q_u = \sum_n q_{ult} A_n \tag{3}$$

Where:
q_{ult} = failure stress;
A_n = area of the n-th helix.

Proceedings of the XXXVIII Iberian Latin-American Congress on Computational Methods in Engineering
P.O. Faria, R.H. Lopez, L.F.F. Miguel, W.J.S. Gomes, M. Noronha (Editores), ABMEC, Florianópolis, SC, Brazil, November 5-8, 2017.

Perko (2009) recommends that the spacing of the piles be adjusted in a way that the capacities calculated from both methods converge, and waste of material for shafts and helical plates may be prevented.

The installation torque method has been put forward by A.B. Chance Company (A.B. Chance, 2014). The method is based on the evidence that the torque measured during installation of the pile indicates the shear resistance of the soil as the helix cuts through (Perko, 2009). A simple empirical correlation between torque and load capacity has been used in this method, as given in Eq. (4) (Mitsch and Clemence, 1985). The torque value T is the mean installation torque corresponding to the final penetration equal to three times the diameter of the largest helix of the pile (Cherry and Souissi, 2010). K_t is the torque correlation factor

$$Q_u = K_t \times T \tag{4}$$

AB Chance (2014) recommends performing load tests to evaluate the helical pile load-displacement behaviour and to estimate the pile load capacity. Stanier et al. (2013) state that full scale load tests are expensive and difficult to perform due to natural variety of subsoil condition. Numerical modelling can be used as a complementary tool for field tests with helical piles. Based on numerical analyses, it is possible to identify an estimate of the shape of the failure surface, establish an idealized failure mechanism, and define the load transfer mechanism from the pile to the soil (Livneh and El Naggar, 2008).

Schiavon (2016) addresses some recommendations that should be taken into account when developing numerical simulations. The installation effect of the pile on the soil was considered by assuming a cylinder of disturbed soil with different properties around the pile axis. According to Salhi (2013), the installation process can cause changes on the specific weight of the soil around the pile. The effect of this change is minimal in cohesive soils and, probably, is more noticeable in loose to medium dense sands, where the void ratio is reduced.

Salhi (2013) analyzed the influence of the spacing ratio s, given by the ratio between the distance between two helical bearing plates and diameter of the lower plate (H_1/D_1), on the load capacity of helical piles and observed a linear relationship between them. Uplift load capacity increases linearly with increases in the spacing ratio. Sprince and Pakrastinsh (2010) performed parametric analyses on helical piles installed in two types of soil: fine sand and a mix of sand, silt and clay. Changes in diameter and installation depth were investigated. The increase of load capacity of a helical pile is influenced by the increase of the plate diameter, but differently depending on each soil. Helical piles showed higher load capacity on soil with high content of silt and clay, when compared with the same piles installed in sand. The authors also verified that increasing the depth of the piles is directly related to the increase in load capacity of the piles.

The objective of this research is to develop and validate a numerical model that can simulate static load tests performed on helical piles installed in sand deposits, and use the model to investigate the effect of geometry parameters on capacity, failure modes, and failure mechanisms of this type of pile.

3. FIELD TESTS USED FOR VALIDATION OF THE NUMERICAL ANALYSIS

The numerical study of this work is based on a series of uplift tests on helical piles, performed in a site located inside the main campus of the Federal University of Rio Grande do

Norte (UFRN) at Natal/RN. The location of the tests inside the site is presented in Fig. 1. Soil samples were collected in the locations indicated in Fig. 1, at the depth of one metre. Figure 1 also shows the position of a standard penetration test performed at the site (SP02).The corresponding soil profile based on bore log SP02 is shown in Fig. 2. The groundwater table was not found. Laboratory test results from the samples indicate the following for layer 1: maximum void ratio = 0.85, minimum void ratio = 0.62, specific unit weight = 26.3 kN/m^3, coefficient of uniformity = 1.92, coefficient of curvature = 0.97, mean particle diameter (D_{50}) = 0.260 mm.

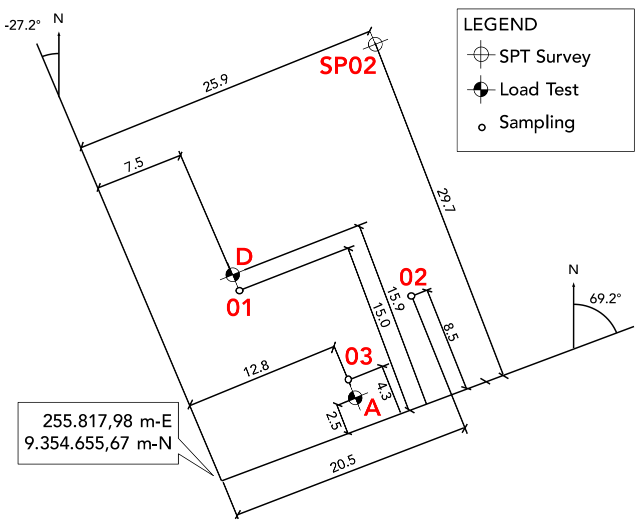

Figure 1. Location of the SPT borehole, the load tests, and the sample collections.

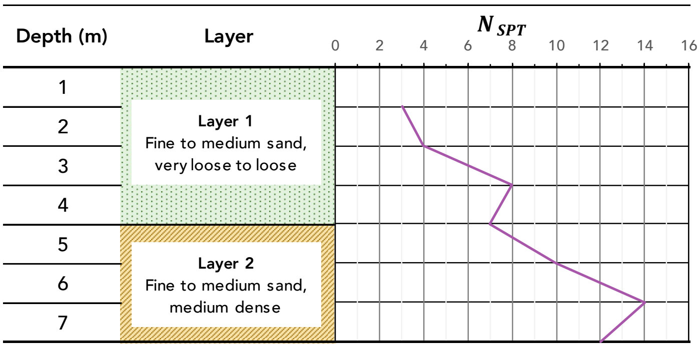

Figure 2. Soil profile obtained from borehole SP02.

Figure 3 shows the prototype helical pile used in the uplift tests. The helical pile consisted of a steel tube with external diameter of 73.0 mm and three helical bearing plates with diameters of 250, 300 and 350 mm. All helices have a pitch of 75.0 mm. The total length of the pile is 5690 mm. The pile was installed in the ground by rotation of the steel tube. The pile reached a depth of installation of about 4 metres.

Four uplift load tests were performed in the field according to ASTM D3689 – 07. Further information on the setup and performance of the field load tests can be obtained in Costa (2017). The results from the load tests were used as a reference to validate the numerical models developed for this work.

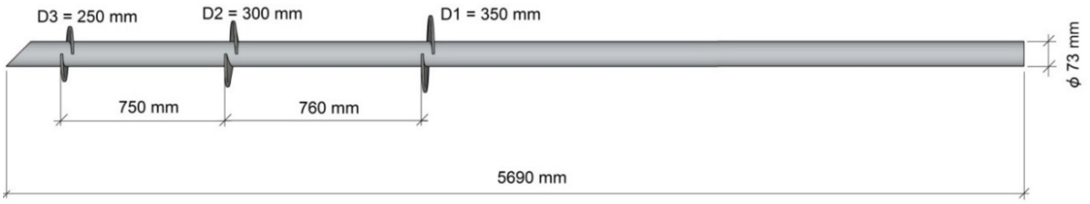

Figure 1. Geometry of the pile used in the field tests. Not to scale.

4. CHARACTERISTICS OF THE NUMERICAL SIMULATIONS

The numerical simulations were conducted using the finite element code Plaxis 2D (2016 version). Figure 4 shows the finite element mesh used in the numerical model, which was conceived by taking into account the axis-symmetry of the problem. The modelled structure consists of a soil mass with longitudinal cross-section of 10 m x 10 m. These dimensions were assumed sufficient to avoid boundary effects. Fixities are used to restrict vertical and horizontal displacements at the lower border and horizontal displacements at the lateral borders. The mesh of the model consists of triangular elements with 15 nodes (Figure 4a). Refining of the mesh within the zone of disturbed soil around the pile was necessary for increasing the accuracy of the results (Figure 4b). The geometry of the pile in the numerical model followed the same geometry of the prototype pile used in the field tests.

The effect of pile disturbance in the ground was considered with the use of a cylinder of soil around the pile, to which specific soil properties were assigned. The disturbed zone around the pile was assumed equal to the radius of the larger pile plus 30 mm, as observed in excavations of the ground performed after the field tests (Costa, 2017).

The behaviour of the pile material was assumed to be linear, since the low level of stresses in the pile during the tests did not cause yielding. The properties used for the steel are in accordance with Brazilian standard NBR 8800. The following values were assumed for the Young's modulus, the Poisson ratio and the specific unit weight of the steel, respectively: 210,000 MPa, 0.3, and 78 kN/m^3.

In the numerical analysis, the two soil layers shown in Fig. 2 were combined into a single layer of undisturbed soil with medium relative density. Figure 4 shows the finite element mesh used in the analysis. Two distinct zones were considered: a zone representing the undisturbed soil mass (purple zone in Fig. 4), and zone representing the disturbed soil close to the pile (green zone in Fig. 4). Estimate of the properties of the purple zone was based on the soil characterization results. The material assigned to this zone was a sand with reduced stiffness and strength parameters. Small cohesion values were used to simulate the suction observed in the field. The parameters for the two soil zones, obtained from the validation process, are shown in Table 1.

The Hardening Soil constitutive model, which is a type of hyperbolic model, was used to simulate the soil behavior. Interface elements were used to simulate the contact between the pile material and the disturbed soil. Mohr-Coulomb failure criterion is assigned as the constitutive model of the elements. Strength degradation at the interface is controlled by parameter R_{inter}, which represents the ratio between the friction at the interface and the internal friction of the soil, as expressed in Eq. (5). The value of R_{inter} was defined as 0.67 in this study. The stiffness of the interface was assumed equal to the stiffness of the soil.

Proceedings of the XXXVIII Iberian Latin-American Congress on Computational Methods in Engineering
P.O. Faria, R.H. Lopez, L.F.F. Miguel, W.J.S. Gomes, M. Noronha (Editores), ABMEC, Florianópolis, SC, Brazil, November 5-8, 2017.

$$R_{inter} = \frac{\tan \phi_{inter}}{\tan \phi'} \quad (5)$$

Table 1. Soil parameters applied to the Hardening Soil constitutive model

Parameter	Undisturbed soil	Disturbed soil
E_{50}	50,000	25,000
υ	0.300	0.200
m	0.500	0.500
ϕ'	37.0°	35.0°
c'	5.0	1.0
ψ	7.0°	5.0°
K_0	0.398	0.426
γ_{unsat}	17.0	16.0

Note: E_{50}= reference Young's modulus for loading (kPa); υ = Poisson's ratio; m = power for stress-level dependency of stiffness; ϕ' = effective friction angle; c' = cohesion (kPa); ψ = dilatancy angle; K_0 = coefficient of lateral stress; γ_{unsat} = unsaturated weight (kN/m^3).

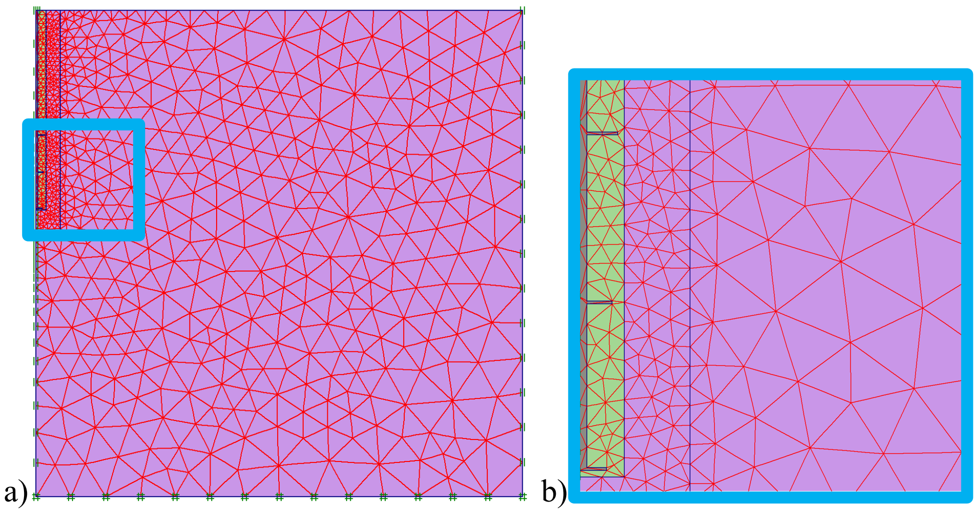

Figure 4. Screenshots from Plaxis 2D: (a) mesh characteristics; (b) mesh detail.

Calculation steps in the numerical model were set to reproduce the sequence of application of the load in the field tests, and included the following: (1) generation of initial stresses in the soil mass; (2) installation of the pile – the material inside the geometric limits of the pile initially filled with undisturbed soil was replaced by the pile material (steel), and the interfaces between the pile and the soil were activated; (3) application of the loading – a vertical distributed uplift loading is activated at the top of the pile.

The parametric study was based on variations of the baseline pile geometry (prototype geometry), which included the diameter of the helical plates, the spacing between the plates and

Proceedings of the XXXVIII Iberian Latin-American Congress on Computational Methods in Engineering
P.O. Faria, R.H. Lopez, L.F.F. Miguel, W.J.S. Gomes, M. Noronha (Editores), ABMEC, Florianópolis, SC, Brazil, November 5-8, 2017.

the depth of installation. All parametric analyses were developed under the same framework conditions for loading, material characteristics, mesh refinement, interface properties, etc.

The effected caused by changes in the diameter of the piles was studied according to two distinct configurations. In one configuration, the three helical plates were assigned the same diameter, which was varied from 200 mm to 400 mm. The other configuration, which correspond to that used in the field tests, the bearing plates were assigned with decreasing diameters. The following sets of helical plate diameters were used, from top to bottom: (1) 250 mm, 200 mm, and 150 mm; (2) 300 mm, 250 mm, and 200 mm; (3) 350 mm, 300 mm, and 250 mm; (4) 400 mm, 350 mm, and 300 mm; and (5) 450 mm, 400 mm, 350 mm.

Changes in spacing between helices were evaluated for s/D_{lower} ratios of 2.0, 2.5, 3, 3.5, 4.0, 4.5, and 5.0 (s is the distance between contiguous helices and D_{lower} is the diameter of the lower helix.)

Effects of depth of pile installation were investigated for the helix configuration of the baseline pile. The following pile lengths were used: 2.0, 2.5, 3.0, 3.5, 4.0, 5.5, and 6.5 m, which correspond, respectively, to the following ratios between depth of the upper helix and its diameter (H_1/D_1): 1.2, 2.8, 4.3, 5.8, 7.3, 11.4, and 14.3.

5. MODEL VALIDATION RESULTS AND FAILURE MECHANISMS

A numerical model of the load tests performed on the prototype pile was developed using Plaxis according to the procedures described previously. The model was based on the geometrical properties of the tests and on the material properties previously described. Preliminary simulations were performed to adjust the input parameters. The curve obtained from the simulation using the parameters from test A is shown in Fig. 5. The simulated response is similar to the experimental results. The agreement between the responses is partly due to the used of the "Hardening Soil" material model, which reproduces the progressive elastic-plastic behaviour observed in the experimental results in sand, with better accuracy than the model with Mohr-Coulomb failure criterion.

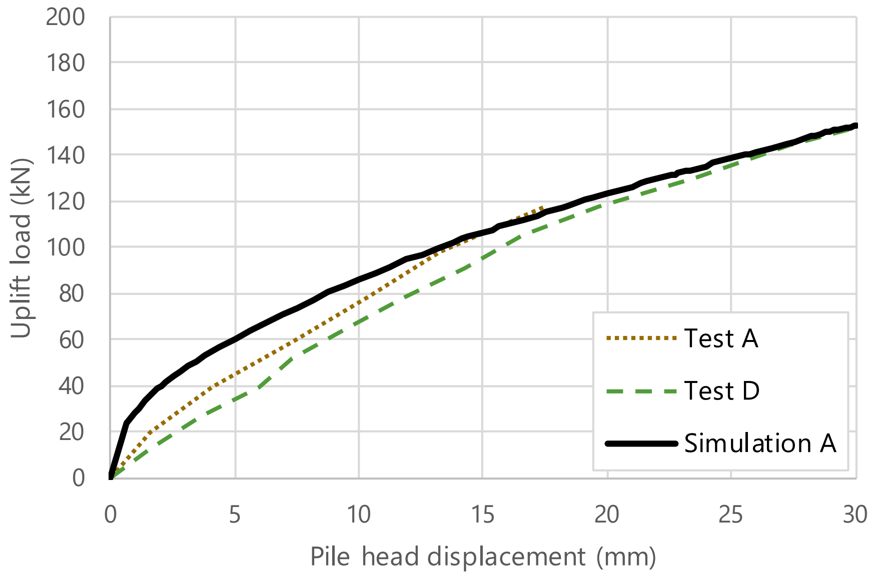

Figure 5. Load-displacement response from field tests and from the numerical simulation of test A.

Figure 6 shows the vertical displacements, the vertical normal stresses and the shear strains inside the soil mass obtained from the simulation of test A. In Fig. 6a it can be observed that the depth where the upper helical plate was installed, 2.57 metres, corresponding to an embedment ratio (H_1/D_1) of 7.3, ensured the failure surface did not extended to the surface, a behaviour referred as deep anchor condition in the literature (Das, 1990; Perko, 2009). Figure 6b shows that the top and the bottom helical bearing plates are subjected to high stresses and the middle plate is only moderately loaded. This indicates that the spacing between the top and the middle helices was sufficiently large to allow the full development of the failure mechanism in the middle helix. As can be observed in Fig. 6c, the shear strains extend from the middle to the top helix. The simulations suggest the load capacity mechanism of the middle helical plate developed through a tapered cylindrical shear surface. Figure 6b shows the bottom helix is subjected to high stresses and Figure 6c shows that shear strains did not extended to the helix above, suggesting the spacing ratio allowed the helix to develop its capacity individually. The spacing ratio in the middle helix was around 2.5 while the ratio in the middle helix is 3.0. Lutenegger (2011) observed the transition between individual plate behaviour and cylindrical shear behaviour in sand occurs at a spacing ratio of about 3. The value is also considered a standard in the pile manufacturing industry (A.B. Chance, 2014). The figures also show that all failure mechanisms were developed inside the zone containing material disturbed by the installation of the helical pile. Schiavon (2016) conducted numerical simulations and field tests and observed similar results.

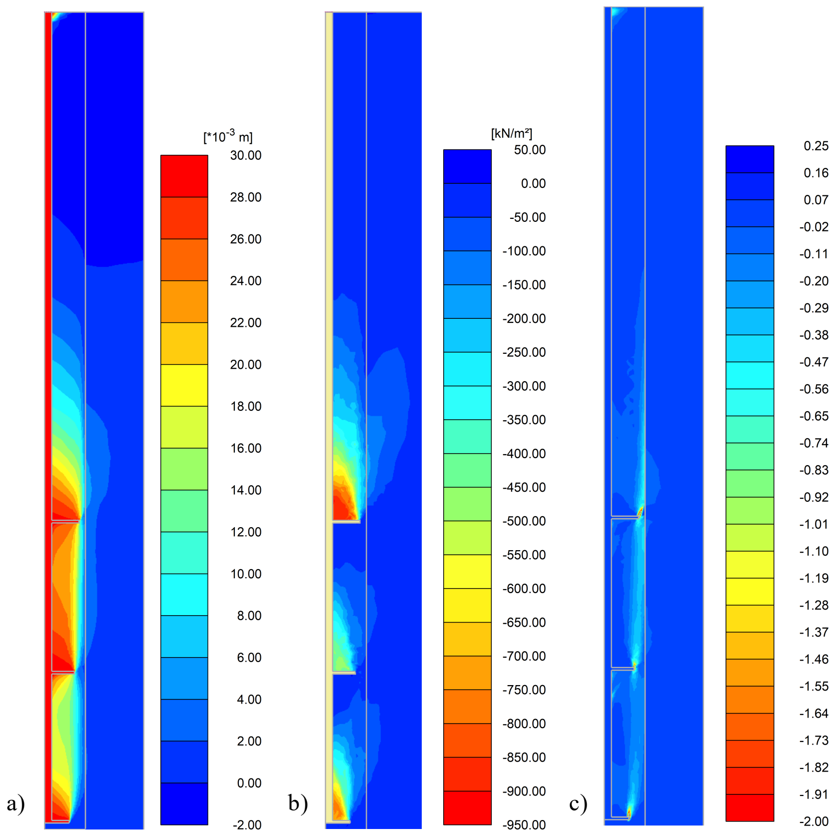

Figure 6. Output results from the simulation of test A: (a) vertical displacements; (b) vertical effective stresses; (c) shear strains.

6. PARAMETRIC STUDY

Parametric analyses were also performed with the developed numerical model. The objective of the parametric analysis is to understand how variations in the design parameters affect the pile uplift capacity and the distribution of loads and stresses around the pile. The ultimate uplift capacity was found according to the modified Davisson criterion (ICC-ES, 2007).

6.1. Relative Embedment Ratio

A range of embedment ratios, H_1/D_1, was simulated and the ultimate uplift capacity obtained from the results is plotted in Fig. 7. The uplift capacity improves with increasing embedment ratio. H_1/D_1 = 7.3 represents the condition of the baseline test and is represented by a dashed line. An increase in uplift capacity on the order of 50 % is observed as the depth ratio is duplicated, for depth ratios above 4.3. Zhang (1999) observed increases in uplift capacity of around 90 % for an increase of 130% in the embedment ratio.

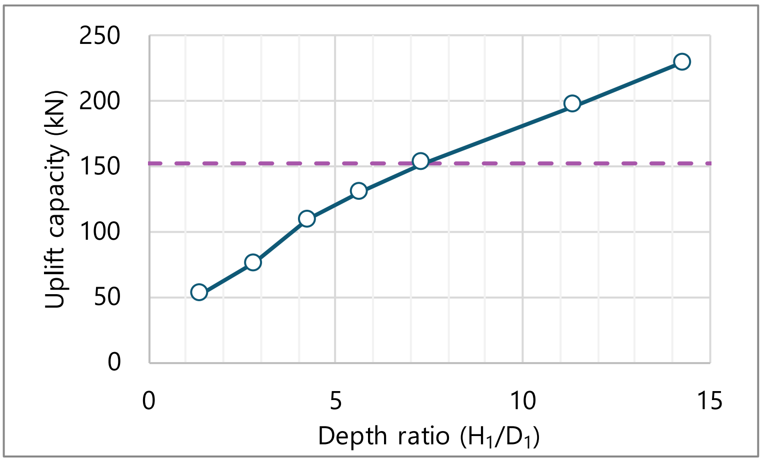

Figure 7. Uplift capacity as a function of embedment ratio (H_1/D_1).

Vertical displacements inside the soil mass, shown in Fig. 8, indicate the transition between shallow and deep failure modes as the embedment ratio is increased. In simulations where the depth ratio is equal or smaller than 4.3 (Figs. 8a-c), the contours of displacement extend up to the surface, which means the top plate behaves as a shallow anchor. The gain in uplift capacity is mostly due to the increased weight of the soil in the cylinder above the top plate. The larger depth ratios represented in Figs. 8d-e show displacements caused by the movement of the top helix no longer reach the surface. This feature indicates deep anchor behaviour. Most of the gain in uplift capacity achieved with larger embedment ratios is due to the increased confinement of the soil around each bearing plate. The transition between shallow and deep conditions occurs with an embedment ratio close to 5.7. According to Rao et al. (1993), piles with H_1/D_1 < 2 are shallow installations, piles with 2 < H_1/D_1 < 4 are transitional installations, and piles with H_1/D_1 > 4 are deep installations. Das (1990) proposed a chart to determinate the critical value *of* H_1/D_1 for which the transition between shallow and deep behaviours occurs in cohesionless soils. The ratio obtained from this chart for sands with φ' = 32° is 4.4. According Mitsch and Clemence (1985) the critical H_1/D_1 is 5.

Proceedings of the XXXVIII Iberian Latin-American Congress on Computational Methods in Engineering
P.O. Faria, R.H. Lopez, L.F.F. Miguel, W.J.S. Gomes, M. Noronha (Editores), ABMEC, Florianópolis, SC, Brazil, November 5-8, 2017.

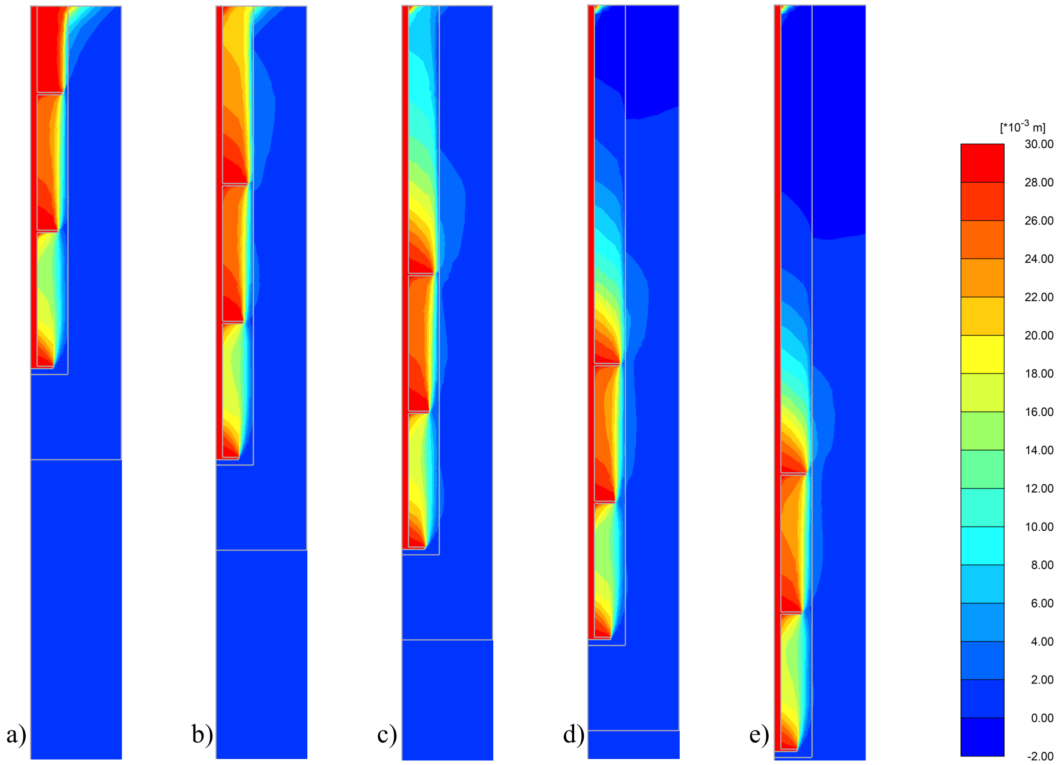

Figure 8. Vertical displacements in piles installed at different depths: a) H_1/D_1 = 1.4; b) H_1/D_1 = 2.8; c) H_1/D_1 = 4.3; d) H_1/D_1 = 5.7; and e) H_1/D_1 = 7.3.

6.2. Helical Plate Diameter

Figure 9 shows the pile uplift capacity obtained with different bearing plate configurations. Variations in the diameter of the bearing plates were simulated in two different ways: (1) with plates with equal diameters (Fig. 9a), and (2) with plates with tapered diameters, i.e., diameters decreasing with increasing depth (Fig. 9b). Combined results of both are shown in Fig. 9c. In Figs. 9a-c, the piles are represented by their average diameter (D_{avg}), e.g. a pile with 250-300-350 mm helices is represented by a D_{avg} = 300 mm. The uplift capacity found in the field (baseline) is highlighted in Figs. 9a-c with a dashed line. It can be observed that increasing diameters in both configurations result in increasing uplift capacities. Figure 9c shows the capacity against mean diameter from both configurations and it is possible to note that tests with equal mean diameter will have similar uplift capacities, regardless of configuration. Another important observation is that doubling the mean diameter results in a capacity increase of, at least, 100%, however, the increased diameter actually represents a fourfold increase in plate area, what can have a significant impact on the cost of the pile.

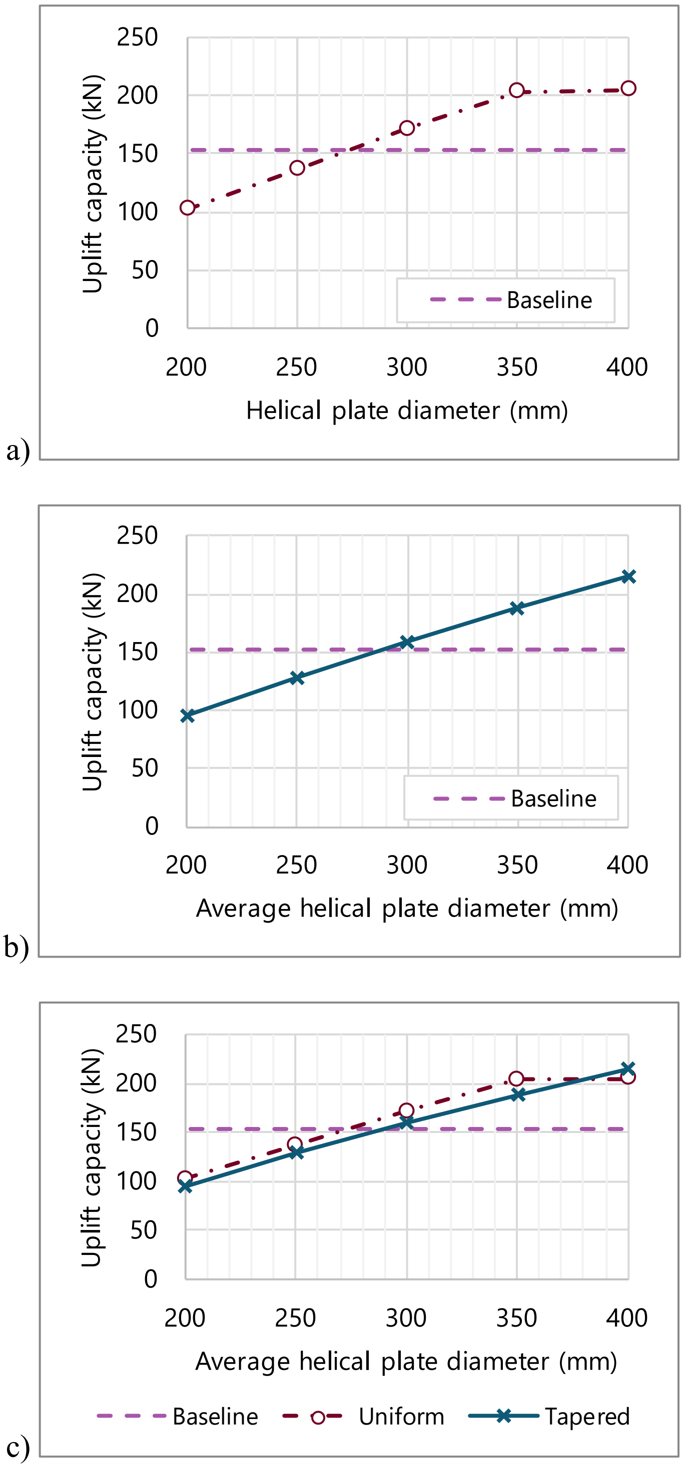

Figure 9. Uplift capacity as a function of helical plate diameter: (a) helices with uniform diameters; (b) helices with tapered diameters; (c) comparison between the two configurations.

6.3. Inter-helix spacing

Inter-helix spacing ratio (s/D_{lower}) is the spacing between two consecutive helical bearing plates divided by the diameter of the lower helix. Ratios between 2 and 4 were simulated with 0.5 interval. The tapered configuration with helix sizes of the baseline field prototype (350-300-250 mm) was used for this investigation. The ultimate capacities obtained from the tests are shown in Fig. 10. The baseline field uplift capacity is indicated in Fig. 10 with a dashed line. Increasing the relative spacing between plates results in gains in uplift capacity until the spacing ratio reaches 4.0. Further increases in spacing will cause the uplift capacity to decrease.

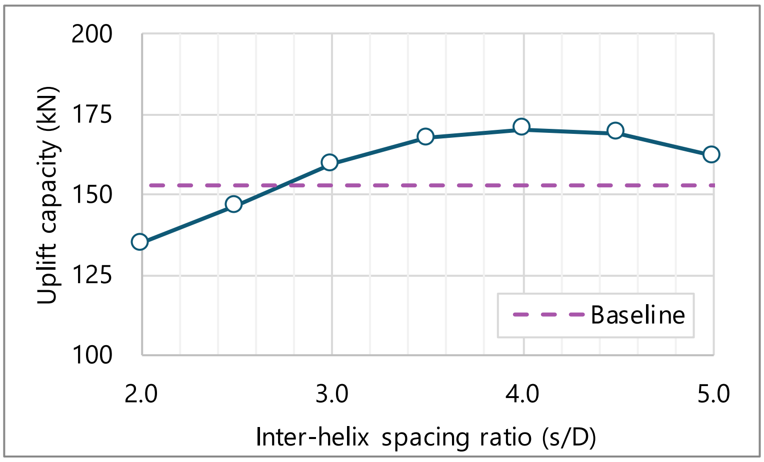

Figure 10. Uplift capacity as a function of inter-helix spacing ratio (s/D_{lower}).

Figure 11 shows the distribution of accumulated shear strain in the soil with increasing spacing ratios. The shear strain in the two lower ratios (Figs 11a-b) starts from the lower plates and reaches the upper plates, revealing a cylindrical shear failure mechanism. A different behaviour can be observed in models with larger s/D_{lower} values. With higher spacing ratios, shear strains start to concentrate closer to the helices, indicating that failure mechanism of the system is partly provided by the individual capacity of the plates (Figs. 11d-g). Even with large relative spacing, the strains still reach the upper helices, however with less intensity. The presence of shear strains extending to the upper helices in piles in these cases can be associated to the lower strength of the soil in the disturbed zone. The test with s/D_{lower} = 3.0 (Fig. 11c) represents the transition from cylindrical shear to individual capacity mechanisms. The result is consistent with optimal spacing ratio used in industry practice (A.B. Chance, 2014). Lutenegger (2011) also observed this transition with the same spacing ratio.

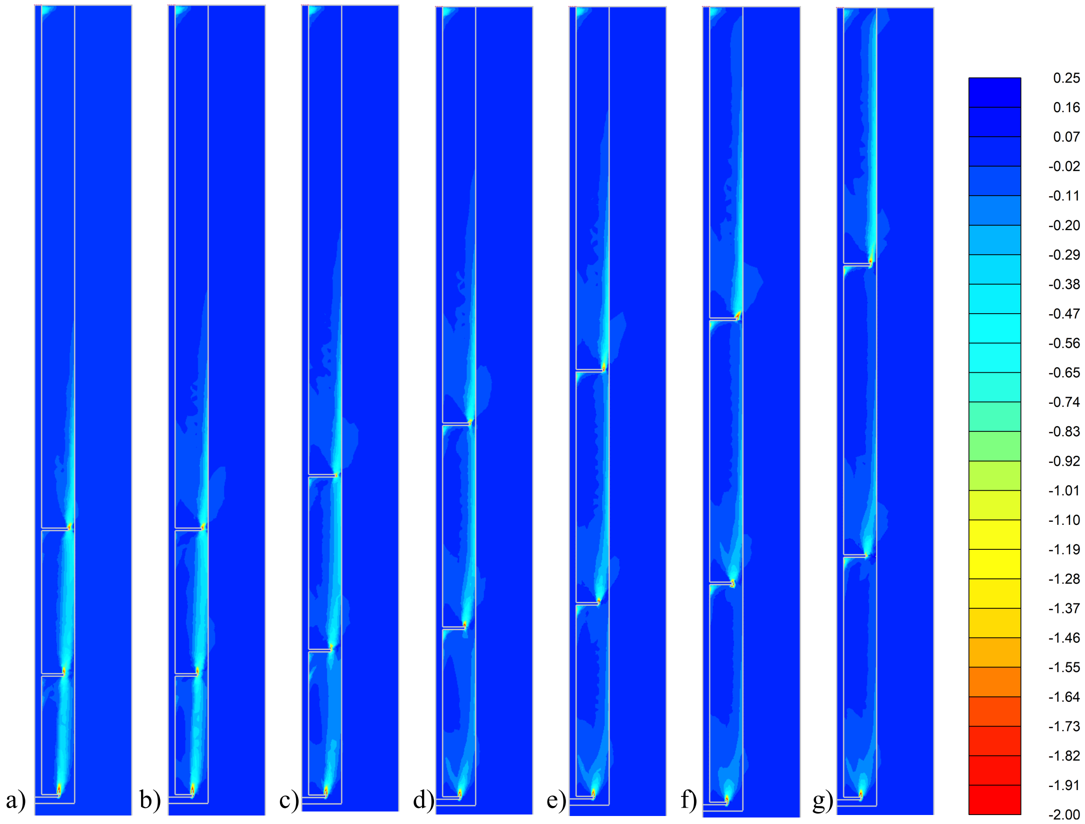

Figure 11. Shear strains in the soil mass with increasing spacing ratios: a) s/D_{lower} = 2.0; b) s/D_{lower} = 2.5; c) s/D_{lower} = 3.0; d) s/D_{lower} =3.5; e) s/D_{lower} = 4.0; f) s/D_{lower} = 4.5; and e) s/D_{lower} = 5.0.

Figure 12 shows the vertical stresses developed in the soil mass with increasing spacing ratios. In Figs. 12a-b, the stresses acting on the top helical plate are clearly higher than the stresses acting on the two lower plates, indicating the failure mechanism of the two lower plates is not fully developed. That is, the load acting on the two lower helices is being resisted by the shear stresses developed around the surface of the cylinder formed around between the uppermost and the lowermost plates, as observed in Fig. 11. Stresses on other piles (Figs. 12c-e) are more evenly distributed between the plates, indicating that their individual capacities are more developed. This means the load transfer mechanism occurs individually and not along a cylindrical shear surface. The stresses on the top helix in Figs. 11f-g are lower than that of the other two helices, showing that increasing the spacing ratio without increasing depth reduces the embedment ratio of the top helix, causing the reductions in uplift capacity observed in Fig. 10.

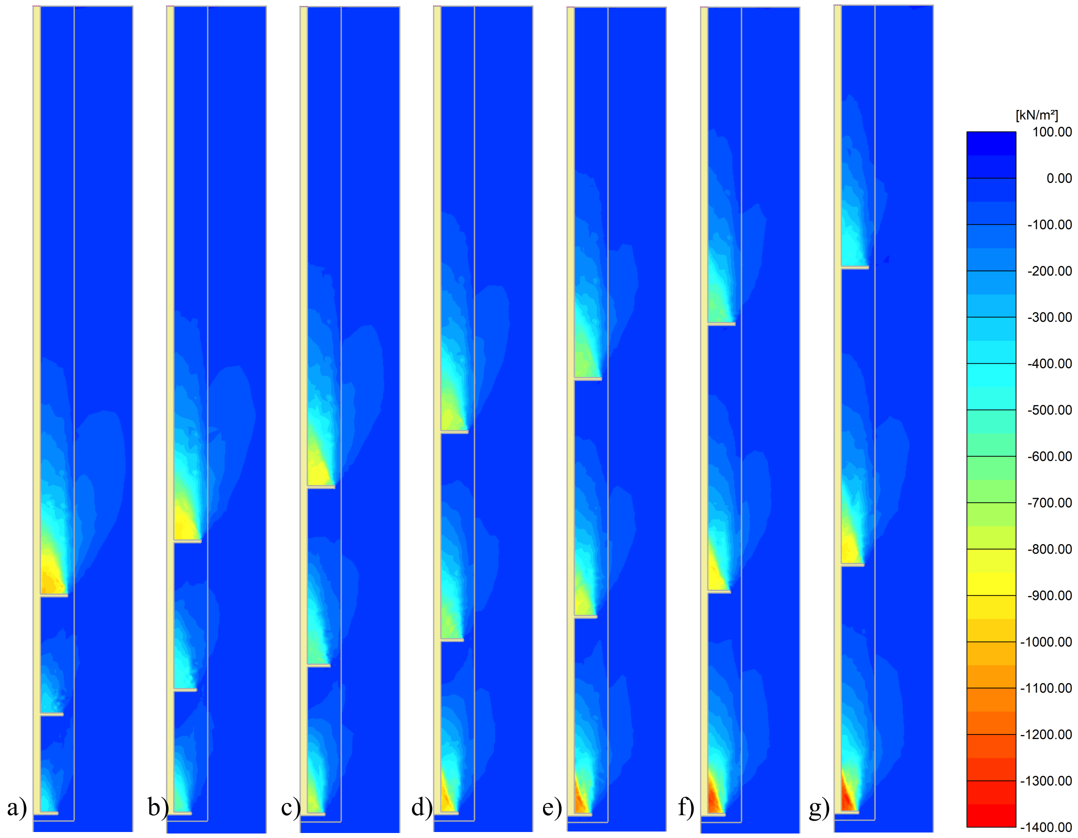

Figure 12. Vertical stresses in the soil mass with increasing spacing ratios: a) s/D_{lower} = 2.0; b) s/D_{lower} = 2.5; c) s/D_{lower} = 3.0; d) s/D_{lower} =3.5; e) s/D_{lower} = 4.0; f) s/D_{lower} = 4.5; and e) s/D_{lower} = 5.0.

7. CONCLUSIONS

A finite element numerical investigation simulating uplift load tests of helical piles installed in a pure sand deposit was presented in this paper. The purpose of the present study is to investigate how specific geometric features of the pile affect the uplift capacity of the system and the corresponding failure mechanisms. The results of the numerical study were validated against results from uplift tests on helical piles performed in the field. The output from the finite element software gave insight into the development of stresses and strains within the soil mass. The following conclusions can be drawn from the obtained results:

a) The uplift capacity of the pile can be improved by increasing the installation depth in deposits of homogenous soil. The capacity increases differently depending on the failure mode of the pile. For piles in the shallow anchor behaviour, increasing the depth increases the load above the upper helix, enabling it to develop its full capacity. As the depth increases, the failure mode transitions to deep anchor behavior and the gain in capacity is due to the improved soil confinement around the helical plates. In the simulations, it was observed that piles with a length of 3.0 m or less, equivalent to depth ratios equal or smaller than 4.3, failed in shallow anchor mode, while deep anchor mode was observed in piles longer than 3.0 m.

b) It was observed that pile uplift capacity increases nearly linearly with increasing mean helical plate diameter. Uniform and tapered plate configurations yielded similar results.
c) Increasing inter-helix spacing increases the uplift capacity due to the transfer of the load from the top helical bearing plate to the middle and bottom plates. Moreover, increasing inter-helix spacing was observed to promote a transition in the failure mechanism from cylindrical shear to individual bearing.
d) Based on the simulations, it can be concluded that the optimal pile geometry should have plates with an average diameter of 350 mm and a spacing ratio between 3.0 and 4.0, ensuring the embedment ratio is equal or higher than 5.7.

Acknowledgements
The author acknowledges the Brazilian funding agency CNPq for the support provided for this research.

REFERENCES

A. B. Chance Co., 2014. Technical Design Manual. 3. ed. Atlas, Hubbel. Centralia, Missouri. 414 p.

Associação Brasileira De Normas Técnicas NBR 8800: projeto de estruturas de aço e de estruturas mista de aço e concreto de edifícios. Rio de Janeiro, 2008.

ASTM D3689/D3689M-07 e1., 2013. Standard Test Methods for Deep Foundations Under Static Axial Tensile Load. *ASTM International*. West Conshohocken, PA. www.astm.org

Cherry, J.; Souissi, M., 2010. Helical pile capacity to torque ratios, current practice, and reliability. *GeoTrends*. pp. 43-52.

Costa, J. P. da S. 2017. Uplift behaviour of helical piles in sand subjected to static and quasi-static cyclic loading. Master's Thesis – Department of Civil Engineering, Centre of Technology, Federal University of Rio Grande do Norte. 118 pp.

Clemence, S. P.; Crouch, L. K.; Stephenson. R. W., 1994. Prediction of uplift capacity for helical anchors in sand. Proceedings of 2nd GeotechnicaL Engineering Conference, Cairo.

Das, B. M., 1990. Earth Anchors. Elsevier Science Publisher. New York. 241 pp.

ICC-Evaluation Services. 2007. AC358 Acceptance Criteria for Helical Pile Foundations and Devices. www.icc-es.org.

Kulhawy, F. H., 1985. Uplift behavior of shallow soil anchors: an overview. Uplift behavior of anchor foundations in soil. *Proceedings of a session sponsored by the Geotechnical Engineering Division of the American Society of Civil Engineers in conjunction with the ASCE Convention in Detroit*, Michigan. pp. 1-25.

Livneh, B.; El Naggar, M. H., 2008. Axial testing and numerical modeling of square shaft helical piles under compressive and tensile loading. *Canadian Geotechnical Journal*. 45(8), pp. 1142-1155.

Lutenneger, A.J., 2011. Behavior of multi-helix screw anchors in sand. *Proceedings of the 14th Pan-American Conference on Soil Mechanics and Geotechnical Engineering*, Toronto.

Mitsch, M.P.; Clemence, S.P., 1985. The uplift capacity of helix anchors in sand. Uplift behavior of anchors foundations in soil. *Proceedings of a section sponsored by Geotechnical Engineering Division of ASCE in conjunction of ASCE convention in Detroit*. Michigan. pp. 26-47.

Pack, J.S., 2013. Helical foundation and tiebacks: quality control, inspection and performance monitoring. *Proceedings of 28th Annual Conference on Deep Foundations*, DFI. pp. 269 – 284.

Perko, H. 2009. *Helical piles: a practical guide to design and installation.* J. W. Sons, Ed.

Rao, S., Prasad, Y. and Shetty, M., 1991. The behavior of model screw piles in cohesive soils, *Soils and Foundations*, 31, pp. 35–50.

Salhi, Lakhdar et al., 2013. Numerical modeling of single helical pile behavior under compressive loading in sand. *Electronic Journal Of Geotechnical Engineering.* French Guiana. pp. 4321-4338.

Schiavon, J. A., 2016. *Comportamento de ancoragens helicoidais submetidas a carregamentos cíclicos*. PhD thesis, University of São Paulo and Nantes Angers and Le Mans University, São Carlos.

Spagnoli, G., 2013. Some considerations regarding the use of helical piles as foundation for offshoe structures. *Soil Mechanics and Foundation Engineering*. 50(3): 102-110.

Stanier, S. A., Black, J. A. & Hird, C. C., 2013. Modelling helical screw piles in soft clay and design implications. *Proceedings of the Institution of Civil Engineers - Geotechnical Engineering*. pp. 447-460.

Stephenson, R. W., 2002. Helical foundations and tie backs: state of the art. University of Missouri-Rolla.

Sprince, A.; Pakrastinsh, L., 2010. Helical pile behaviour and load transfer mechanism in different soils. *The 10th International Conference*. pp. 1174-1180.

Tsuha, C. H. C., 2007. Modelo teórico para controle da capacidade de carga à tração de estacas metálicas helicoidais em solo arenoso. São Carlos, SP. PhD thesis – University of São Paulo. 245 pp.

Zhang, D., 1999. *Predicting capacity of helical screw piles in Alberta soils.* MSc Thesis, University of Alberta, Edmonton.